Reprinted from June 1985, Vol. 107, Journal of Applied Mechanics

A Beam Theory for Anisotropic Materials

O. A. Bauchau
Assistant Professor,
Department of Mechanical Engineering,
Aeronautical Engineering and Mechanics,
Rensselaer Polytechnic Institute,
Troy, N.Y. 12181

Beam theory plays an important role in structural analysis. The basic assumption is that initially plane sections remain plane after deformation, neglecting out-of-plane warpings. Predictions based on these assumptions are accurate for slender, solid, cross-sectional beams made out of isotropic materials. The beam theory derived in this paper from variational principles is based on the sole kinematic assumption that each section is infinitely rigid in its own plane, but free to warp out of plane. After a short review of the Bernoulli and Saint-Venant approaches to beam theory, a set of orthonormal eigenwarpings is derived. Improved solutions can be obtained by expanding the axial displacements or axial stress distribution in series of eigenwarpings and using energy principles to derive the governing equations. The improved Saint-Venant approach leads to fast converging solutions and accurate results are obtained considering only a few eigenwarping terms.

1 Introduction

Timoshenko beam theory is well known by structural designers and is widely used as a first approximation in numerous structural applications. For solid cross-sectional beams made out of isotropic materials, this theory gives accurate predictions for aspect ratios $L/h \gtrsim 5$ (L is the span of the beam and h its height). Because it is based on the assumption that cross sections remain plane after deformation, the theory predicts a linear distribution of axial strains. However, additional axial strains are induced by warping incompatibilities generated either by specific loading or boundary conditions, or by the occurrence of nonuniform torsion or bending. According to Saint-Venant's Principle these additional strains tend to decay away from the perturbation that created them. The decay length δ is defined as the distance it takes for these strains to decay to a neglectible value. For solid cross-sectional beams made out of isotropic materials, this decay length is of the order of the height of the beam, i.e., $\delta \simeq h$. A physical meaning of the validity range of the theory is found by rewriting it as $L/\delta \gtrsim 5$, stating that the span of the beam must be large compared to the perturbed zone δ.

In the case of thin-walled box beams, it was recognized early that beam theory was only a poor approximation, because warping and shear lag effects are significant for those structures. Von Karman and Chien [1] gave a solution to this problem using a system of orthogonal states of stress. Argyris and Dunne [2] derived solutions for more general problems and showed the existence of fast converging series based on a similar system of orthogonal stress states.

More recently, with the increasing use of composite materials, Saint-Venant's principle has been investigated theoretically for anisotropic elasticity [3, 4]. The decay length δ was found to be proportional to $\sqrt{E/G}$ (E is the longitudinal Young's modulus and G the shear modulus). This means that for highly anisotropic materials the decay length can be much larger than for isotropic materials. Goetschel [5] calculated these decay length for different beams made out of composite materials. For a thin-walled rectangular cross-section δ is found to be $7h$, and for an I cross section $\delta = 15h$. Beam theory can still be applied if $L/\delta \gtrsim 5$, i.e., $L/h \gtrsim 35$ and 75, respectively. Needless to say, such a restriction makes beam theory inapplicable to practical structures.

The purpose of this paper is to derive a beam theory that can be used when only the geometric condition $L/h \gtrsim 5$ is satisfied.

2 Geometry Assumptions

Thin-walled box beams with closed cross sections will be considered (see Fig. 1). The contour of the section (denoted $\mathcal{C}$) is a parametric function of the variable s, while the variable z

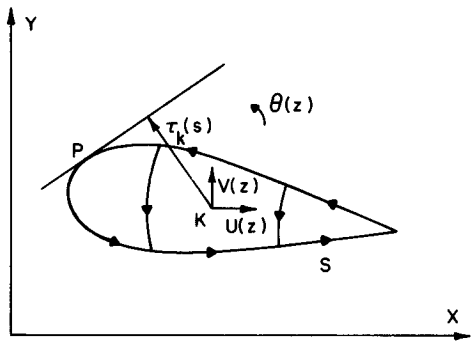

Fig. 1 Geometry of a typical cross section

Contributed by the Applied Mechanics Division for publication in the JOURNAL OF APPLIED MECHANICS.
Discussion on this paper should be addressed to the Editorial Department, ASME, United Engineering Center, 345 East 47th Street, New York, N.Y. 10017, and will be accepted until two months after final publication of the paper itself in the JOURNAL OF APPLIED MECHANICS. Manuscript received by ASME Applied Mechanics Division, April, 1984; final revision, August, 1984.

runs along the span of the beam. The basic assumption is that each section is infinitely rigid in its own plane, but free to warp out of plane. This assumption has two important implications: (*i*) the inplane displacements of the section are fully represented by three rigid body modes $u(z)$, $v(z)$, $\theta(z)$, respectively, the two translations and the rotation of the section, and (*ii*) any applied transverse load only induces membrane stresses in the structure, specifically an axial stress flow n, and a shear stress flow q. For thin walled beams these two stress flows are uniform across the thickness and the other stress components are assumed to be neglectible.

Finally, we must specify the stress-strain relations: the materials is either isotropic or curvilinear orthotropic with the axes of orthotropy parallel to the axis of the beam and the tangent to the cross-sectional curve, so that:

$$n = A_{nn}\epsilon \tag{1}$$

$$q = A_{qq}\gamma \tag{2}$$

A_{nn} and A_{qq} are the elastic coefficients (see Appendix *B*); ϵ is the axial strain, and γ the shear strain. They are related to the displacements by

$$\epsilon = \frac{\partial w}{\partial z} \tag{3}$$

$$\gamma = \frac{\partial w}{\partial s} + u'\frac{dx}{ds} + v'\frac{dy}{ds} + \theta'\tau_k \tag{4}$$

where w is the axial displacement, $\tau_k(s)$ is the distance from the center K to the tangent to the cross-sectional curve (see Fig. 1), and $(\,)'$ means derivative with respect to z.

3 The Bernoulli Solution

Bernoulli's beam theory is based on the additional assumption that cross sections remain plane after deformation, implying a linear axial displacement:

$$w(s,z) = Z(z) + (x-x_n)X(z) + (y-y_n)Y(z) \tag{5}$$

where $Z(z)$ is a uniform extension of the section, $X(z)$, $Y(z)$ are the rotations of the section, and x_n, y_n are the coordinates of the neutral axis.

It is convenient to derive the equations of the problem from energy principles; in this case we must minimize the total potential energy π,

$$\pi = \frac{1}{2}\int_0^L\int_\zeta (A_{nn}\epsilon^2 + A_{qq}\gamma^2)dsdz - \int_0^L (p_x u + p_y v + m\theta)dz \tag{6}$$

where p_x, p_y are the applied transverse loads per unit span in the x and y directions, respectively, and m is the applied torque per unit span.

Using the basic assumption (5) and the strain definitions (3) and (4) we find,

$$\epsilon = Z' + (x-x_n)X' + (y-y_n)Y' \tag{7}$$

$$\gamma = (X+u')\frac{dx}{ds} + (Y+v')\frac{dy}{ds} + \theta'\tau_k \tag{8}$$

The total potential energy (6) now becomes

$$\pi = \frac{1}{2}\int_0^L [SZ'^2 + I_{xx}X'^2 + I_{yy}Y'^2 + 2I_{xy}X'Y' + A_{xx}(X+u')^2 + A_{yy}(Y+v')^2 + 2A_{xy}(X+u')(Y+v') + I_p\theta'^2]dz - \int_0^L (p_x u + p_y v + m\theta)dz \tag{9}$$

where $S = \int_\zeta A_{nn}\,ds$ is the axial stiffness; $I_{xx} = \int_\zeta A_{nn}(x-x_n)^2 ds$ is the bending stiffness (similar definitions for I_{yy} and I_{xy}), $A_{xx} = \int_\zeta A_{qq}(dx/ds)^2$ is the shear stiffness (similar definitions for A_{yy} and A_{xy}), and $I_p = \int_\zeta A_{qq}\tau_k^2\,ds$ is the torsional stiffness.

The location of the shear center K was chosen to decouple bending and torsion by setting

$$\int_C A_{qq}\tau_k\frac{dx}{ds}ds = \int_C A_{qq}\tau_k\frac{dy}{ds}ds = 0 \tag{10}$$

This gives a pair of linear equations for the coordinates x_k, y_k of the shear center. The Bernoulli solution is obtained by minimizing (9) with respect to the functions X, Y, u, v, θ, Z

$$(I_{xx}X' + I_{xy}Y')'' = -p_x,$$

$$(I_{xy}X' + I_{yy}Y')'' = -p_y \tag{11a}$$

$$[A_{xx}(X+u') + A_{xy}(Y+v')]' = -p_x,$$

$$[A_{xy}(X+u') + A_{yy}(Y+v')]' = -p_y \tag{11.b}$$

$$(I_p\theta')' = -m, \quad (SZ')' = 0 \tag{11.c}$$

This solution takes into account shearing deformations (11.*b*), it is sometimes referred to as Timoshenko beam theory. The solution to equations (11) is summarized here with a subscript "*b*":

$$w_b = Z + (x-x_n)X + (y-y_n)Y, \quad u_b = u$$

$$n_b = A_{nn}(Z' + (x-x_n)X' + (y-y_n)Y'], \quad v_b = v \tag{12}$$

$$q_b = A_{qq}\left[(X+u')\frac{dx}{ds} + (Y+v')\frac{dy}{ds} + \theta'\tau_k\right], \quad \theta_b = \theta.$$

4 The Saint-Venant Solution

The absence of out-of-plane warpings in the Bernoulli approach results in poor accuracy of the solution. In a first attempt to correct this situation Saint-Venant's approach is considered now. The assumption here is that the axial stresses are linearly distributed, i.e.,

$$n(s,z) = A_{nn}[A(z) + (x-x_n)B(z) + (y-y_n)C(z)], \tag{13}$$

in place of equation (5).

The Reissener Principle [6] will be used here to derive the governing equations. With our notations the functional to be minimized reads:

$$\pi_R = \int_0^L\int_\zeta \left[(n\epsilon + q\gamma) - \frac{1}{2}\left(\frac{n^2}{A_{nn}} + \frac{q^2}{A_{qq}}\right)\right]dsdz - \int_0^L (p_x u + p_y v + m)\,dz \tag{14}$$

Using the basic assumption (13) and the strain definitions (3) and (4) it becomes

$$\pi_R = \int_0^L\int_\zeta \left\{A_{nn}[A + (x-x_n)B + (y-y_n)C]\frac{\partial w}{\partial z} + q\left(\frac{\partial w}{\partial z} + u'\frac{dx}{ds} + v'\frac{dy}{ds} + \theta'\tau_k\right) - \frac{1}{2}A_{nn}[A + (x-x_n)B + (y-y_n)C]^2 - \frac{1}{2}\frac{q^2}{A_{qq}}\right\}dsdz - \int_0^L (p_x u + p_y v + m\theta)dz \tag{15}$$

Minimizing first with respect to w and q the following differential system is found:

$$\frac{\partial q}{\partial s} = -A_{nn}[A' + (x-x_n)B' + (y-y_n)C']$$

$$\frac{\partial w}{\partial w} - \frac{q}{A_{qq}} = -u'\frac{dx}{dz} - v'\frac{dy}{dz} - \theta'\tau_k \tag{16}$$

The detailed integration of this system is described in Appendix *A*. The solution (*A*15) is then replaced in the Reissener functional, and the variations on the remaining function u, v, θ, A, B, C yield the complete solution:

$$X' = i_{xx}M_x + i_{xy}M_y, \quad Y' = i_{xy}M_x + i_{yy}M_y$$
$$u' = U_x T_x + U_y T_y - X, \quad v' = V_x T_x + V_y T_y - Y \qquad (17)$$
$$J\theta' = M_k, \quad SZ = N$$

where

$M_x = \int_\zeta n(x-x_n)\,ds$ is the bending moment (similar definition for M_y),

$T_x = \int_\zeta q \frac{dx}{ds}\,ds$ is the shear force (similar definition for T_y),

$M_k = \int_\zeta q\ \tau_k\ ds$ is the torque at the shear center K,

$N = \int_\zeta n\ ds$ is the axial force,

$J = \int_\zeta Q_t\ \tau_k ds$ is the torsional stiffness

i_{xx}, i_{yy}, i_{xy} is the inverse tensor of bending stiffnesses.

Here again the location of the shear center K has been chosen to decouple bending and torsion by setting

$$\int_\zeta Q_1 \tau_k ds = \int_\gamma Q_2 \tau_k ds = 0. \qquad (18)$$

This results in a pair of linear equations for the coordinates of the shear center x_k, y_k. The Saint-Venant solution is now summarized with a subscript "sv":

$$w_{sv} = Z + (x-x_n)X + (y-y_n)Y + W_x T_x + W_y T_y + W_t \frac{M_k}{J},$$

$$n_{sv} = A_{nn}\left\{\frac{N}{S} + [i_{xx}(x-x_n) + i_{xy}(y-y_n)]M_x + [i_{xy}(x-x_n) + i_{yy}(y-y_n)]M_y\right\},$$

$$q_{sv} = Q_x T_x + Q_y T_y + Q_t \frac{M_k}{J},$$
$$u_{sv} = u, \quad v_{sv} = v, \quad \theta_{sv} = \theta. \qquad (19)$$

where the different functions are solutions of the system (17) and W_x, W_y, W_t as well as Q_x, Q_y, Q_t are defined in Appendix A. It is interesting to note that this solution satisfies all the equations of the problem, except the stress strain relation (1).

5 Eigenwarpings

In the Bernoulli solution (12) all warpings are ignored, and the Saint-Venant solution (19) only considers specific warpings (W_x, W_y, W_t). In this section a set of orthonormal warpings is derived. They will be used later for a series expansion of the exact solution. Eigenwarpings are derived from the principle of minimum potential energy (6). An homogeneous problem is considered (i.e., no loading is applied) and a solution of the following form is assumed:

$$w(s,z) = W(s)F(z), \; u'(z) = UF(z),$$
$$v'(z) = VF(z), \; \theta'(z) = \Xi F(z) \qquad (20)$$

$F(z)$ and $W(s)$ are unknown functions of z and s, respectively, U, V, and Ξ are unknown parameters. These assumptions result in expressions for the strains where the variables are separated:

$$\epsilon = W(s)F'(z) \qquad (21)$$

$$\gamma = \left(\frac{dW}{ds} + U\frac{dx}{ds} + V\frac{dy}{ds} + \Xi\tau_k\right)F(z) = \Gamma(s)F(z) \qquad (22)$$

The energy principle (6) now reads:

$$\pi = \frac{1}{2}\int_0^L \int_\zeta (A_{nn}W^2F'^2 + A_{qq}\Gamma^2F^2)ds\,dz \qquad (23)$$

This functional can be first minimized with respect to F, to find

$$F'' - \mu^2 F = 0 \qquad (24)$$

where μ^2 is a yet unknown separation constant. Using this relation the energy principle becomes:

$$\pi = \frac{1}{2}\left[\int_0^L F^2 dz\right]\left[-\mu^2\int_\zeta A_{nn}W^2 ds + \int_\zeta A_{qq}\Gamma^2 ds\right] \qquad (25)$$

This functional is now minimized with respect to the function W and the parameters U, V, and Ξ. This leads to an eigenvalue problem for μ^2, that can be written in the form of a Rayleigh quotient

$$\mu_i^2 = \frac{\int_\zeta A_{qq}\left(\frac{dW_i}{ds} + U_i\frac{dx}{ds} + V_i\frac{dy}{ds} + \Xi_i\tau_k\right)^2 ds}{\int_\zeta A_{nn}W_i^2 ds} \qquad (26)$$

$W_i(s)$ are the eigenwarpings of the problem. A set of orthonormality relationships is associated with this problem:

$$\int_\zeta A_{nn}W_iW_j ds = \delta_{ij}, \quad \int_\zeta A_{qq}\Gamma_i\Gamma_j ds = \mu^2\delta_{ij} \qquad (27)$$

6 Improving the Bernoulli Solution

The Bernoulli solution will be improved by adding to the basic assumption (5), a series expansion in terms of eigenwarpings, and by correcting the other displacements components accordingly (see equation (20)):

$$w(s,z) = w_b + \sum_i w_i(s)F_i(z) \qquad (28.a)$$

$$u' = u'_b + \sum_i U_iF_i(z), \quad v' = v'_b + \sum_i V_iF_i(z),$$

$$\theta' = \theta'_b + \sum_i \Xi_iF_i(z) \qquad (28.b)$$

Note that arbitrary axial displacements can be represented with the preceding series expansion (28.a), so no assumption is made on axial displacements distribution. However, the assumption of infinite inplane rigidity of the section is required to express the inplane displacements (28.b) as functions of z only.

The strains corresponding to this displacement field can be used to evaluate the potential energy (6), and taking into account orthonormality relations (27) it reads:

$$\pi = \pi_b + \sum_i \int_0^L \left[\frac{1}{2}(F_i'^2 + \mu_i^2F_i^2) - d_i\right]dz \qquad (29)$$

where π_b is the potential energy for the Bernoulli solution (9), and

$$d_i = T_xU_i + T_yV_i + M_k\Xi_i \qquad (30)$$

Expression (29) shows the Bernoulli solution to be decoupled from the corrective terms F_i and the different corrective terms decoupled from each other. Minimizing π_b will render the Bernoulli solution (12) and minimizing the corrective terms with respect to F_i gives:

$$F_i'' - \mu_i^2F_i = -d_i \qquad (31)$$

This differential equation is solved readily and yields the

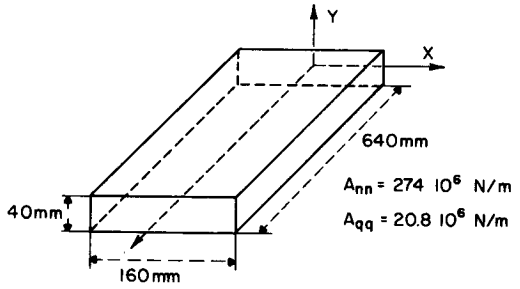

Fig. 2 The thin-walled, rectangular cross-sectional beam analyzed in the numerical example

solution of the problem as a series expansion of eigenwarpings:

$$w = w_b + \sum_i W_i F_i \quad u' = u_b' + \sum_i U_i F_i$$

$$n = n_b + \sum_i A_{nn} W_i F_i' \quad v = v_b + \sum_i V_i F_i \tag{32}$$

$$q = q_b + \sum_i A_{qq} \Gamma_i F_i \quad \theta' = \theta_b' + \sum_i \Xi_i F_i$$

When infinite series are used, equations (32) give the exact solution of the problem under the sole assumption of infinite inplane rigidity of the section.

7 Improving the Saint-Venant Solution

Following a similar procedure, the Saint-Venant solution is improved by adding to the basic assumption (13) a series expansion in terms of eigenwarpings.

$$n(s,z) = n_{sv} + \sum_i A_{nn} W_i(s) K_i(z) \tag{33}$$

The Reissener principle (14) is used here again to derive the solution. The system of two differential equations resulting from the variations on w and q is integrated as previously for the terms pertaining to the basic Saint-Venant solution (see Appendix A). The remaining terms of the system can be identified as the Euler equations of the functional (25) which are satisfied by all eigenwarpings. The complete solution to this system is then placed into the functional (15) which becomes

$$\pi_R = \pi_{Rsv} + \sum_i \int_0^L \left(-\frac{1}{2} \frac{K_i'^2}{\mu_i^2} - \frac{1}{2} K_i^2 + \frac{d_i'}{\mu_i^2} K_i \right) dz \tag{34}$$

where π_{Rsv} is the Reissner functional for the Saint-Venant solution (15). Here again the basic solution is decoupled from the corrective terms, as are the different corrective terms from each other. Minimization of π_{Rsv} will render the Saint-Venant solution (19) and minimization of the corrective terms with respect to K_i gives

$$K_i'' - \mu_i^2 K_i = -d_i' \tag{35}$$

The solution of this simple differential equation gives the solution of the problem as

$$w = w_{sv} + \sum_i \frac{W_i}{\mu_i^2} K_i' \quad u' = u_{sv}' + \sum_i \frac{U_i}{\mu_i^2} K_i'$$

$$n = n_{sv} + \sum_i A_{nn} W_i K_i \quad v' = v_{sv}' + \sum_i \frac{V_i}{\mu_i^2} K_i' \tag{36}$$

$$q = q_{sv} + \sum_i A_{qq} \frac{\Gamma_i}{\mu_i^2} K_i' \quad \theta' = \theta_{sv}' + \sum_i \frac{\Xi_i}{\mu_i^2} K_i'$$

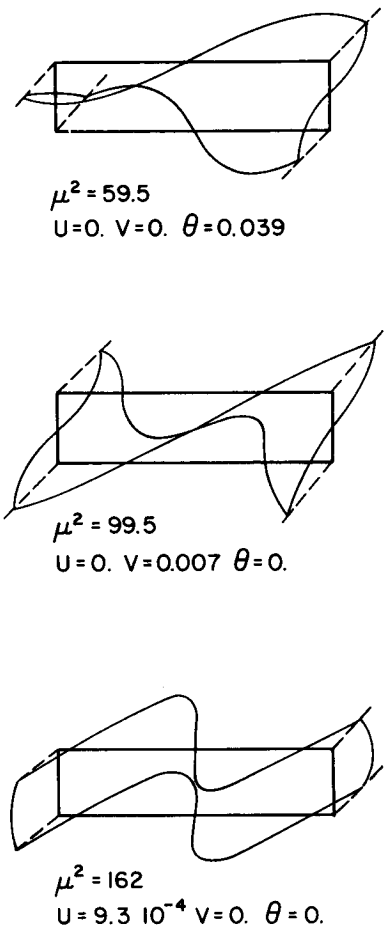

Fig. 3 A few eigenwarpings of the rectangular section

For infinite series, equation (36) give the exact solution to the problem, again under the assumption of infinite inplane rigidity of the section. Solution (32) is based on an assumed displacement approach and yield a lower bound of the strain energy if a truncated series expansion is used. On the other hand, solution (36) is based on an assumed equilibrating stress field yielding an upper bound of the strain energy for truncated series expansion.

8 Numerical Examples

A specific example is treated here, using the different approaches described in the previous sections. Figure 2 depicts the thin-walled, rectangular cross-sectional beam to be analyzed. The aspect ratio $L/h = 4$. The first step is to calculate the eigenwarpings W_i and the associated eigenvalues μ_i. The eigenvalue problem (26) can be solved using a finite element technique where the function W is discretized over the section. Then, a standard subspace iteration method allows the calculation of the eigenvalues and eigenwarpings. For this example, 36 nodal points were used to model the section and 24 eigenwarpings were extracted. The first few modes are shown in Fig. 3. If the beam is subjected to a uniform load p_o in the y direction, the differential equation (31) to be solved for the improved Bernoulli approach is

$$F_i'' - \mu_i^2 F_i = -p_0 V_i (L - z)$$

Boundary conditions at $z = 0 \quad F_i = 0$; at $z = L \; F_i' = 0$

This equation is readily integrated to give the final solution (32). In particular the tip deflection of the beam is found to be:

Table 1 Numerical results for the different approaches

	Tip deflection $\frac{V_{tip}}{p_0 L^4}$ [10^{-6}m]		Tip twist $\frac{\theta_{tip}}{m_0 L^4}$ [10^{-6}]	
	"Bernoulli"	"Saint-Venant"	"Bernoulli"	"Saint-Venant"
Euler	3.29	3.29		
Shear	0.734	1.57	91.70	143.3
	$\Delta = 19\%$		$\Delta = 44\%$	
1st term	0.446	−0.160	20.65	−9.90
2nd term	0.104	−0.0176	10.05	−2.10
3rd term	0.0283	−0.00311	3.57	−0.463
4th term	0.00229	−0.000186	0.722	−0.067
Total	4.604	4.677	126.7	130.
	$\Delta = 1.5\%$		$\Delta = 3\%$	

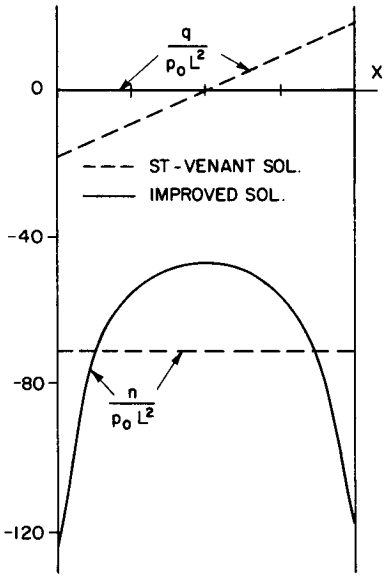

Fig. 4 Stress distributions in the upper skin of the beam (root section) under uniform transverse load p_0

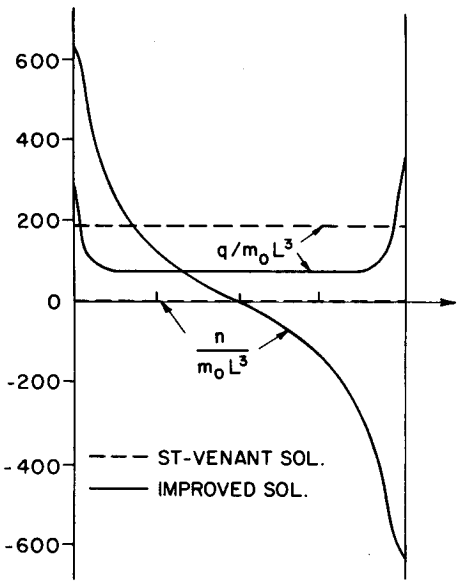

Fig. 5 Stress distributions in the upper skin of the beam (root section) under uniform torque m_0

$$\frac{v_{tip}}{P_0 L^4} = \frac{1}{8I_{yy}} + \frac{1}{2L^2 A_{yy}} + \sum_i \left(\frac{V_i}{\mu_i L}\right)^2 \left[\frac{1}{2} + \frac{1}{\mu_i^2 L^2} - \frac{1+\mu_i L sh\mu_i L}{\mu_i^2 L^2 ch\mu_i L}\right] \tag{37}$$

The first term represents the bending deflection, the second term is the shearing deflection, and the summation represents the corrective deflections due to the different eigenwarping terms. Alternatively the improved Saint-Venant approach requires to solve equation (35),

$$K_i'' - \mu_i^2 K_i = p_0 V_i$$

Boundary conditions at $z=0$ $K_i' = -p_0 L V_i$; at $z=L$ $K_i = 0$

From the general solution (36) the tip deflection is now

$$\frac{v_{tip}}{p_0 L^4} = \frac{1}{8I_{yy}} + \frac{V_y}{2L^2} + \sum_i \left(\frac{V_i}{\mu_i^2 L^2}\right)^2 \left[1 - \frac{1+\mu_i L \text{sh}\mu_i L}{\text{ch}\mu_i L}\right] \tag{38}$$

Table 1 lists the numerical results for the two approaches. A comparison between the basic Bernoulli and Saint-Venant solutions shows a discrepancy of 20 percent. After adding three corrective terms this discrepancy is reduced to about 1 percent, showing that both solutions have converged. It is important to note the excellent convergence rate of the Saint-Venant approach in $(1/\mu_i L)^4$ versus $(1/\mu_i L)^2$ for the Bernoulli approach. Considering one term only in the improved Saint-Venant approach leads to a solution acceptable for engineering purposes. It should be noted here that according to (26), the eigenvalues μ_i are proportional to $\sqrt{A_{qq}/A_{nn}}$. Thus the magnitude of the corrective terms in the improved Saint-Venant approach is proportional to $(A_{nn}/A_{qq})^2$ resulting in large corrections for highly anisotropic materials.

If the beam is subjected to a uniform torque m_0, the tip twist $\theta_{tip}/m_0 L^4$ can be calculated in a similar fashion. The tip twist are $1/2I_p L^2$ and $1/2JL^2$ for the basic Bernoulli and Saint-Venant approaches, respectively. The corrective terms are identical to those in (37) and (38) except that V_i is replaced by Ξ_i. The results are summarized in Table 1 and show a 44 percent discrepancy for the basic solutions. The corrective terms reduce this discrepancy to about 3 percent. Again the Saint-Venant approach shows a better convergence rate; two corrective terms are necessary here to obtain an accurate solution.

It is also interesting to compute the stress distribution at the root of the beam. Figure 4 shows the distribution of axial stresses $n/p_0 L^2$ and shear stess $q/p_0 L^2$ in the upper face of the beam under a uniform loading p_0, using the improved Saint-Venant approach (36). Instead of the uniform axial stress predicted by the basic theory, a large shear lag effect is

observed. Figure 5 depicts the stress distributions when the loading is a uniformly distributed torque m_0. Here the uniform shear stress distribution predicted by the basic theory is significantly altered and large axial stresses are generated near the corners of the section.

9 Conclusion

Two approaches for an improved beam theory have been developed, consisting both of a series expansion of the exact solution in terms of eigenwarpings. The Saint-Venant approach shows an excellent convergence rate and for a specific example two terms of the series were shown to give accurate results.

Instead of solving the differential equations (31) or (35) exactly, a finite element approach is possible. The energy principles (29) or (34) can be used to derive the stiffness matrices for improved beam elements.

This theory is not limited to thin-walled box beams. In the case of solid cross sections, the concept of eigenwarpings can be extended as long as the basic assumption remains valid, i.e., as long as the section can be assumed infinitely rigid in its own plane. Once the eigenwarpings are found, the solutions (32) or (36) remain valid.

Acknowledgments

This research was supported by NASA and AFOSR under NASA Grant NGL 33-018-003, Dr. M. Greenfield and Dr. A. Amos are technical monitors, in the respective agencies.

References

1 Von Karman, Th., and Chien, W. Z., "Torsion With Variable Twist," *Journal of the Aeronautical Sciences*, Vol. 13, No. 10, Oct. 1946, pp. 503–510.

2 Argyris, J. H., and Dunne, P. C., "The General Theory of Cylindrical and Conical Tubes Under Torsion and Bending Loads," *J. of Royal Aero. Soc.*, Vol. 51, 1947, pp. 199–269; 757–784; 844–930.

3 Horgan, C. O., "On Saint-Venant's Principle in Plane Anisotropic Elasticity," *J. of Elasticity*, Vol. 2, 1972, pp. 169–180.

4 Choi, I., and Horgan, C. O., "Saint-Venant's Principle and End Effects in Anisotropic Elasticity," ASME JOURNAL OF APPLIED MECHANICS, Vol. 44, 1977, pp. 424–430.

5 Goetschel, D. B., and Hu, T. H., "Quantification of Saint-Venant's Principle for a General Prismatic Member," ASME JOURNAL OF APPLIED MECHANICS, to appear.

6 Reissener, E., "On a Variational Theorem in Elasticity," *J. of Math. and Phys.*, Vol. 29, No. 22, July 1950, pp. 90–95.

7 Tsai, S. W., and Hahn, H. T., *Introduction to Composite Materials*, Technonic, 1980.

APPENDIX A

In developing the Saint-Venant theory, the differential system (16) must be integrated. The solution for $w(s,z)$ consists of a linear part (identical to the Bernoulli solution) plus an additional warping function $g(s,z)$:

$$w(s,z)=Z(z)+(x-x_n)X(z)+(y-y_n)Y(z)+g(s,z) \quad (A1)$$

Considering at first the B' term only at the right-hand side of the system and introducing (A1) gives

$$\frac{\partial q}{\partial s}=-A_{nn}(x-x_n)B'$$

$$\frac{\partial}{\partial s}[g+(x-x_n)(u'+X)+(y-y_n)(v'+Y)+Z]$$

$$-\frac{q}{A_{qq}}=0 \quad (A2)$$

The following type of solution is expected:

$$q(s,z)=Q(s)B' \quad g(s,z)=W(s)B'$$
$$u'+X=UB', \quad v+Y=VB', \quad Z=aB', \quad (A3)$$

which reduce the system (A2) to:

$$\frac{dQ}{ds}=-A_{nn}(x-x_n)$$

$$\frac{d\rho}{ds}-\frac{Q}{A_{qq}}=0 \quad (A4)$$

where

$$\rho(s)=W(s)+U(x-x_n)+V(y-y_n)+a \quad (A5)$$

System (A4) can be integrated now since s is the only variable left. Alternatively it is readily verified that (A4) are the Euler equations of the following functional

$$\pi_1=\frac{1}{2}\int_\zeta A_{qq}\left(\frac{d\rho_1}{ds}\right)^2 ds-\int_\zeta A_{nn}(x-x_n)\rho_1 ds \quad (A6)$$

The solution ρ_1 minimizes π_1, then successively

$$Q_1(s)=A_{qq}\frac{d\rho_1}{ds} \quad (A7)$$

and

$$W_1(s)=\rho_1-U_1(x-x_n)-V_1(y-y_n)-a_1 \quad (A8)$$

Finally W_1 is enforced to be a warping by setting

$$\int_\zeta A_{nn}W_1 ds=\int_\zeta A_{nn}(x-x_n)W_1 ds$$

$$=\int_\zeta A_{nn}(y-y_n)W_1 ds=0 \quad (A9)$$

these three relations are used to calculate a_1, U_1, and V_1.

In a second step we consider only the C' term in (16). Following the same procedure as in the foregoing, the solution ρ_2 is found from minimizing

$$\pi_2=\frac{1}{2}\int_\zeta A_{qq}\left(\frac{d\rho_2}{ds}\right)^2 ds-\int_\zeta A_{nn}(y-y_n)\rho_2 ds \quad (A10)$$

$Q_2(s)$ and $W_2(s)$ then follow like in (A7) and (A8). In a last step, the θ' term in (16) is integrated. Following once again a similar procedure, the system now reduces to

$$\frac{dQ}{ds}=0$$

$$\frac{d\rho}{ds}-\frac{Q}{Aqq}=-\rho_k$$

The equation can be integrated directly or show to be equivalent to the minimization of

$$\pi_t=\frac{1}{2}\int_\zeta A_{qq}\left(\frac{d\rho_t}{ds}\right)^2 ds+\int_\zeta A_{qq}\tau_k\left(\frac{d\rho_t}{ds}\right)ds \quad (A12)$$

and finally

$$Q_t=A_{qq}\left(\frac{d\rho_t}{ds}+\tau_k\right) \quad (A13)$$

and

$$W_t=\rho_t-U_t(x-x_n)-V_t(y-y_n)-a_t$$

The complete solution of system (16) is obtained by adding the different contributions:

$$q(s,z)=Q_1B'+Q_2C'+Q_t\theta'$$
$$w(s,z)=Z(z)+(x-x_n)X(z)+(y-y_n)Y(z)$$
$$+W_1B'+W_2C'+W_t\theta'$$
$$u'=U_1B'+U_2C'+U_t\theta'-X$$
$$v=V_1B'+V_2C'+V_t\theta'-Y \quad (A15)$$

In later developments it will be convenient to use linear combinations of these solutions, for instance

$$Q_x = i_{xx}Q_1 + i_{xy}Q_2 \quad (A16)$$

$$Q_y = i_{xy}Q_1 + i_{yy}Q_2 \quad (A16)$$

W_x, W_y; U_x, U_y and V_x, V_y can be defined similarly.

APPENDIX B

The inplane stiffness of an orthotropic laminate can be written in matrix form as [7]:

$$\begin{bmatrix} n \\ n_t \\ q \end{bmatrix} = \begin{bmatrix} A_{11} & A_{12} & A_{16} \\ A_{21} & A_{22} & A_{26} \\ A_{61} & A_{62} & A_{66} \end{bmatrix} \begin{bmatrix} \epsilon \\ \epsilon_t \\ \lambda \end{bmatrix} \quad (B1)$$

where n_t and ϵ_t are the stress and strain in the direction tangent to the cross-sectional curve. The assumption of infinite inplane rigidity of the cross section allows to set $n_t \simeq 0$ so that $B1$ reduces to:

$$\begin{bmatrix} n \\ q \end{bmatrix} = \begin{bmatrix} A_{nn} & A_{nq} \\ A_{nq} & A_{qq} \end{bmatrix} \begin{bmatrix} \epsilon \\ \lambda \end{bmatrix} \quad (B2)$$

where

$$A_{nn} = A_{11} - A_{12}^2/A_{22}, \quad A_{qq} = A_{66} - A_{26}^2/A_{22},$$

$$A_{nq} = A_{16} - A_{12}A_{26}/A_{22} \quad (B3)$$

when the material is isotropic, an orthotropic with the axes of orthotropy parallel to the axis of the beam and the tangent to the cross-sectional curve, we have $A_{16} = A_{26} = 0$, thus $A_{nq} = 0$ and equations (32) are decoupled as (1) and (2).

observed. Figure 5 depicts the stress distributions when the loading is a uniformly distributed torque m_0. Here the uniform shear stress distribution predicted by the basic theory is significantly altered and large axial stresses are generated near the corners of the section.

9 Conclusion

Two approaches for an improved beam theory have been developed, consisting both of a series expansion of the exact solution in terms of eigenwarpings. The Saint-Venant approach shows an excellent convergence rate and for a specific example two terms of the series were shown to give accurate results.

Instead of solving the differential equations (31) or (35) exactly, a finite element approach is possible. The energy principles (29) or (34) can be used to derive the stiffness matrices for improved beam elements.

This theory is not limited to thin-walled box beams. In the case of solid cross sections, the concept of eigenwarpings can be extended as long as the basic assumption remains valid, i.e., as long as the section can be assumed infinitely rigid in its own plane. Once the eigenwarpings are found, the solutions (32) or (36) remain valid.

Acknowledgments

This research was supported by NASA and AFOSR under NASA Grant NGL 33-018-003, Dr. M. Greenfield and Dr. A. Amos are technical monitors, in the respective agencies.

References

1 Von Karman, Th., and Chien, W. Z., "Torsion With Variable Twist," *Journal of the Aeronautical Sciences*, Vol. 13, No. 10, Oct. 1946, pp. 503–510.

2 Argyris, J. H., and Dunne, P. C., "The General Theory of Cylindrical and Conical Tubes Under Torsion and Bending Loads," *J. of Royal Aero. Soc.*, Vol. 51, 1947, pp. 199–269; 757–784; 844–930.

3 Horgan, C. O., "On Saint-Venant's Principle in Plane Anisotropic Elasticity," *J. of Elasticity*, Vol. 2, 1972, pp. 169–180.

4 Choi, I., and Horgan, C. O., "Saint-Venant's Principle and End Effects in Anisotropic Elasticity," ASME JOURNAL OF APPLIED MECHANICS, Vol. 44, 1977, pp. 424–430.

5 Goetschel, D. B., and Hu, T. H., "Quantification of Saint-Venant's Principle for a General Prismatic Member," ASME JOURNAL OF APPLIED MECHANICS, to appear.

6 Reissener, E., "On a Variational Theorem in Elasticity," *J. of Math. and Phys.*, Vol. 29, No. 22, July 1950, pp. 90–95.

7 Tsai, S. W., and Hahn, H. T., *Introduction to Composite Materials*, Technonic, 1980.

APPENDIX A

In developing the Saint-Venant theory, the differential system (16) must be integrated. The solution for $w(s,z)$ consists of a linear part (identical to the Bernoulli solution) plus an additional warping function $g(s,z)$:

$$w(s,z)=Z(z)+(x-x_n)X(z)+(y-y_n)Y(z)+g(s,z) \quad (A1)$$

Considering at first the B' term only at the right-hand side of the system and introducing (A1) gives

$$\frac{\partial q}{\partial s}=-A_{nn}(x-x_n)B'$$

$$\frac{\partial}{\partial s}[g+(x-x_n)(u'+X)+(y-y_n)(v'+Y)+Z]$$

$$-\frac{q}{A_{qq}}=0 \quad (A2)$$

The following type of solution is expected:

$$q(s,z)=Q(s)B' \quad g(s,z)=W(s)B'$$
$$u'+X=UB', \quad v+Y=VB', \quad Z=aB', \quad (A3)$$

which reduce the system (A2) to:

$$\frac{dQ}{ds}=-A_{nn}(x-x_n)$$

$$\frac{d\rho}{ds}-\frac{Q}{A_{qq}}=0 \quad (A4)$$

where

$$\rho(s)=W(s)+U(x-x_n)+V(y-y_n)+a \quad (A5)$$

System (A4) can be integrated now since s is the only variable left. Alternatively it is readily verified that (A4) are the Euler equations of the following functional

$$\pi_1=\frac{1}{2}\int_\zeta A_{qq}\left(\frac{d\rho_1}{ds}\right)^2 ds-\int_\zeta A_{nn}(x-x_n)\rho_1 ds \quad (A6)$$

The solution ρ_1 minimizes π_1, then successively

$$Q_1(s)=A_{qq}\frac{d\rho_1}{ds} \quad (A7)$$

and

$$W_1(s)=\rho_1-U_1(x-x_n)-V_1(y-y_n)-a_1 \quad (A8)$$

Finally W_1 is enforced to be a warping by setting

$$\int_\zeta A_{nn}W_1 ds=\int_\zeta A_{nn}(x-x_n)W_1 ds$$

$$=\int_\zeta A_{nn}(y-y_n)W_1 ds=0 \quad (A9)$$

these three relations are used to calculate a_1, U_1, and V_1.

In a second step we consider only the C' term in (16). Following the same procedure as in the foregoing, the solution ρ_2 is found from minimizing

$$\pi_2=\frac{1}{2}\int_\zeta A_{qq}\left(\frac{d\rho_2}{ds}\right)^2 ds-\int_\zeta A_{nn}(y-y_n)\rho_2 ds \quad (A10)$$

$Q_2(s)$ and $W_2(s)$ then follow like in (A7) and (A8). In a last step, the θ' term in (16) is integrated. Following once again a similar procedure, the system now reduces to

$$\frac{dQ}{ds}=0$$

$$\frac{d\rho}{ds}-\frac{Q}{Aqq}=-\rho_k$$

The equation can be integrated directly or show to be equivalent to the minimization of

$$\pi_t=\frac{1}{2}\int_\zeta A_{qq}\left(\frac{d\rho_t}{ds}\right)^2 ds+\int_\zeta A_{qq}\tau_k\left(\frac{d\rho_t}{ds}\right)ds \quad (A12)$$

and finally

$$Q_t=A_{qq}\left(\frac{d\rho_t}{ds}+\tau_k\right) \quad (A13)$$

and

$$W_t=\rho_t-U_t(x-x_n)-V_t(y-y_n)-a_t$$

The complete solution of system (16) is obtained by adding the different contributions:

$$q(s,z)=Q_1B'+Q_2C'+Q_t\theta'$$
$$w(s,z)=Z(z)+(x-x_n)X(z)+(y-y_n)Y(z)$$
$$+W_1B'+W_2C'+W_t\theta'$$
$$u'=U_1B'+U_2C'+U_t\theta'-X$$
$$v=V_1B'+V_2C'+V_t\theta'-Y \quad (A15)$$

In later developments it will be convenient to use linear combinations of these solutions, for instance

Table 1 Numerical results for the different approaches

	Tip deflection $\frac{V_{tip}}{p_0 L^4}$ [10^{-6}m]		Tip twist $\frac{\theta_{tip}}{m_0 L^4}$ [10^{-6}]	
	"Bernoulli"	"Saint-Venant"	"Bernoulli"	"Saint-Venant"
Euler	3.29	3.29		
Shear	0.734	1.57	91.70	143.3
	$\Delta = 19\%$		$\Delta = 44\%$	
1st term	0.446	−0.160	20.65	−9.90
2nd term	0.104	−0.0176	10.05	−2.10
3rd term	0.0283	−0.00311	3.57	−0.463
4th term	0.00229	−0.000186	0.722	−0.067
Total	4.604	4.677	126.7	130.
	$\Delta = 1.5\%$		$\Delta = 3\%$	

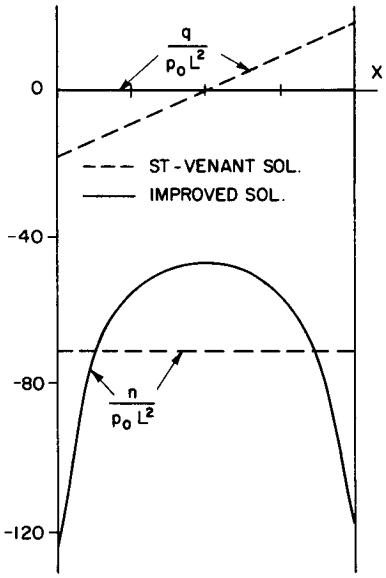

Fig. 4 Stress distributions in the upper skin of the beam (root section) under uniform transverse load p_0

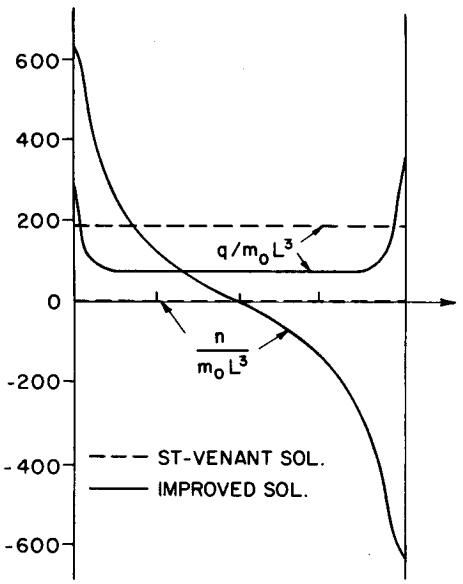

Fig. 5 Stress distributions in the upper skin of the beam (root section) under uniform torque m_0

$$\frac{v_{tip}}{P_0 L^4} = \frac{1}{8I_{yy}} + \frac{1}{2L^2 A_{yy}} + \sum_i \left(\frac{V_i}{\mu_i L}\right)^2 \left[\frac{1}{2} + \frac{1}{\mu_i^2 L^2} - \frac{1+\mu_i L sh\mu_i L}{\mu_i^2 L^2 ch\mu_i L}\right] \tag{37}$$

The first term represents the bending deflection, the second term is the shearing deflection, and the summation represents the corrective deflections due to the different eigenwarping terms. Alternatively the improved Saint-Venant approach requires to solve equation (35),

$$K_i'' - \mu_i^2 K_i = p_0 V_i$$

Boundary conditions at $z=0$ $K_i' = -p_0 L V_i$; at $z=L$ $K_i = 0$

From the general solution (36) the tip deflection is now

$$\frac{v_{tip}}{p_0 L^4} = \frac{1}{8I_{yy}} + \frac{V_y}{2L^2} + \sum_i \left(\frac{V_i}{\mu_i^2 L^2}\right)^2 \left[1 - \frac{1+\mu_i L \text{sh}\mu_i L}{\text{ch}\mu_i L}\right] \tag{38}$$

Table 1 lists the numerical results for the two approaches. A comparison between the basic Bernoulli and Saint-Venant solutions shows a discrepancy of 20 percent. After adding three corrective terms this discrepancy is reduced to about 1 percent, showing that both solutions have converged. It is important to note the excellent convergence rate of the Saint-Venant approach in $(1/\mu_i L)^4$ versus $(1/\mu_i L)^2$ for the Bernoulli approach. Considering one term only in the improved Saint-Venant approach leads to a solution acceptable for engineering purposes. It should be noted here that according to (26), the eigenvalues μ_i are proportional to $\sqrt{A_{qq}/A_{nn}}$. Thus the magnitude of the corrective terms in the improved Saint-Venant approach is proportional to $(A_{nn}/A_{qq})^2$ resulting in large corrections for highly anisotropic materials.

If the beam is subjected to a uniform torque m_0, the tip twist $\theta_{tip}/m_0 L^4$ can be calculated in a similar fashion. The tip twist are $1/2I_p L^2$ and $1/2JL^2$ for the basic Bernoulli and Saint-Venant approaches, respectively. The corrective terms are identical to those in (37) and (38) except that V_i is replaced by Ξ_i. The results are summarized in Table 1 and show a 44 percent discrepancy for the basic solutions. The corrective terms reduce this discrepancy to about 3 percent. Again the Saint-Venant approach shows a better convergence rate; two corrective terms are necessary here to obtain an accurate solution.

It is also interesting to compute the stress distribution at the root of the beam. Figure 4 shows the distribution of axial stresses $n/p_0 L^2$ and shear stess $q/p_0 L^2$ in the upper face of the beam under a uniform loading p_0, using the improved Saint-Venant approach (36). Instead of the uniform axial stress predicted by the basic theory, a large shear lag effect is